



1 **Fish oil in a wave tank: a look at the air-water response**

2

3 Alvis Benetazzo¹, Luigi Cavaleri¹, Hongyu Ma², Shumin Jiang², Filippo Bergamasco³, Wenzheng Jiang², Sheng
4 Chen², Fangli Qiao²

5

6

7 ¹ Istituto di Scienze Marine (ISMAR), Consiglio Nazionale delle Ricerche (CNR), Venice, Italy.

8 ² First Institute of Oceanography (FIO), State Oceanic Administration (SOA), Qingdao, P. R. China.

9 ³ DAIS – Università Ca' Foscari, Venice, Italy.

10

11 *Correspondence to:* A. Benetazzo (alvise.benetazzo@ve.ismar.cnr.it)

12

13 **Abstract.** Surfactant layers with viscoelastic properties floating on the water surface damp short gravity-capillary
14 waves. Inspired by the known virtue of fish oil to still angry seas, a laboratory study has been made on wind wave
15 generation and on the interaction between wind-waves, paddle-waves and airflow in a tank containing a thin fish
16 oil film uniformly spread on the water surface. According to the Marangoni resonance-type damping mechanism,
17 for oily surfaces the energy dissipation process is quite selective in wavenumbers, but its effects are not, since it
18 spreads (although to a lesser extent) towards longer and shorter waves via nonlinear interactions and modification
19 of the airflow profile. With a thin layer of oil on the surface, it is rather peculiar that in the wind-only condition (no
20 paddle waves) the wave field does not grow from the rest condition. This equilibrium was altered by paddle
21 (longer) waves, the generation and evolution of short waves (in clean water and with oil) being modified by their
22 interaction with the orbital velocity of the longer waves and their effect on the airflow. Paddle waves did grow
23 under the action of wind, how much being similar in clean and oily water conditions, a fact we ascribe to the
24 similar distortion of the wind profile in the two cases. We have also found that wind-supported stress on the oily
25 water surface was able to generate a surface current, whose magnitude turns out to be comparable to the one in
26 clean water. Our results expand previous investigations on the same topic. We stress the benefit of experiments
27 with surfactants to explore in detail the physics at, and the exchanges across, the wavy and no-wavy air-water
28 interface.

29 **Keywords:** Wind-wave growth; Fish Oil; Surfactant; Marangoni forces; Paddle waves.



1 **1 Introduction**

2 Wind blowing over the water surface generates wind waves and drift currents. It is instructive that the physics of
3 this evident truth is still a question of debate. One reason is that the implied physics spans a large range of scales,
4 the various processes interacting among them, and possibly hiding the reasons of that behavior. Nature offers a full
5 panorama of events at all the possible scales. However, it is mainly in the laboratory that we can explore, also with
6 the desired repetitiveness, the details of some, albeit limited in scale, processes. Indeed this approach has provided
7 in time enlightening findings to be then used in the daily operational activities. Already in the '70s and '80s
8 Mitsuyasu, in a series of remarkable papers, provided basic hints into the generative and dissipative processes of
9 wind waves (see, among others, Kusaba and Mitsuyasu, 1984; Mitsuyasu, 1966; Mitsuyasu and Honda, 1982,
10 1986). Mark Donelan, using data first from a tower in lake Ontario and then in a laboratory wind wave tunnel in
11 Miami, provided basic hints in several aspects of wind wave generation (see e.g. Donelan, 1990). In more recent
12 times, following a very sophisticated and detailed series of experiments, Buckley and Veron (2016) have provided
13 a detailed description of the air flow during wave generation. The specific problem of the trigger of the initial
14 wavelets has been dealt with by Kawai (1979), van Gastel et al. (1985), and more recently by Liberzon and Shemer
15 (2011) and Zavadsky and Shemer (2017).

16 A problem that (in most of the cases) does not concern the open ocean is how air and sea interact when the
17 water surface is covered by a thin layer of surface active agent. This physical aspect has been early dealt with
18 experimentally in studies by Hühnerfuss et al. (1981) and Mitsuyasu and Honda (1986). The interest is not only on
19 the results of the experiments, but on the physics they reveal and the considerations they allow on the general
20 problem of wind wave generation. Following this logical link we have carried out a series of experiments aimed at,
21 if not solving the whole problem (a daunting task), at least shading new light on some of its aspects. Science
22 proceeds often by negations. New results may not only hint in one direction, but also exclude a solution, in so
23 doing helping focusing along the right path.

24 In the following we describe what has been done, for each experiment stressing the doubts and the
25 implications. Given that a large part of what was done deals with fish oil on the surface, following subsection 1.1
26 provides a compact, but sufficient for the purpose, description of the related physics. The general description of the
27 experimental set-up is in section 2, where we also list the general plan of the experiments and the finally available



1 data. The actual technical description of the results of the experiments are in section 3, the whole then discussed in
2 section 4, and summarized and itemized in the final section 5.

1.1 A little physics on the interaction between oil slick and gravity-capillary waves

3 It is well known that the addition of a thin film (from 10^{-9} to 10^{-8} m, almost mono-molecular) of surfactant (blend
4 of *surface active agent*) to the water surface has a intense effect on the energy of the gravity-capillary waves by
5 altering the surface tension at the water-air interface (Fiscella et al., 1985). Oil has been used for centuries to
6 smooth the sea surface, so much that expressions as “to pour oil on troubled water” have acquired a more general
7 meaning. See later in the paper the impressive example reported by Cox et al. (2017). Crucial in this respect is the
8 type of oil, in particular its polarity. Mineral oils, so often wrongly used during the Second World War, are not
9 effective because their molecules tend to group together in a heap. On the contrary the polar molecules of fish, and
10 partly also vegetable, oils repel each other. Hence, once poured on water, they tend to distribute rapidly on the
11 available surface acquiring a quasi-monomolecular level. Known since ancient time, this effect was first studied in
12 the 19th century by the Italian physicist Carlo Marangoni, hence the official name of the process (Marangoni,
13 1872). In relatively recent times the first report of Marangoni damping of wave spectra came from Cini et al.
14 (1983) who had noted the effect in the polluted (although by mineral oils) water in the gulf of Genoa, Italy.
15 However, clear evidence of Marangoni damping on slick-covered ocean waves was first presented by Ermakov et
16 al. (1985, 1986) during field experiment in the Black Sea.

17 This resonance-type Marangoni damping (to be soon described) can be effective for surface waves in two
18 possible conditions. The first one is in the open ocean, in which an existing wind-forced wave field travels trough a
19 surfactant patch, with the consequent possibility of detection (lack of return signal) by microwave radars (Feindt,
20 1985). The second one, typical of laboratory experiments, is where the wind blows over a water surface
21 homogeneously covered (since the rest condition) with a surfactant film. The latter is the one we dealt with in the
22 experiments described in this study.

23 The presence of an extremely thin (practically mono-molecular) layer of oil on the surface strongly affects
24 the air-sea interaction. In this respect, it is generally agreed that, in clean water, the growth of the first detectable
25 ripples on the water surface is rather well explained by the effect of air turbulence advected by the wind (Phillips,
26 1957). That process is quickly overtaken as the waves grow by the feedback caused by the wave-induced pressure
27 oscillations in the air, as soon as the airflow vertical profile is modified by waves. Miles (1957) proposed a wave



1 growth mechanism that accounts for this change. This theory was extended and later applied by Janssen (1991) to
2 wave forecasting. Its validity is questioned for very short waves whose phase speed is as slow as the air friction
3 velocity (Miles, 1993). According to the shear-flow model by Miles, waves with phase speed c grow when the
4 curvature in the vertical wind profile, at the height (called critical height) where the wind speeds equals c , is
5 negative. As a result, the wind profile changes because of the continuous transfer of energy to the waves (Janssen,
6 1982). The growth rate is proportional to this curvature and it has an implicit dependence on the roughness length
7 on the wavy water surface. Hence any modification of the vertical wind shear modifies the momentum transfer
8 from wind to waves. This equilibrium is altered for slick-covered surfaces.

9 The physics of the Marangoni effect is thought to be well understood, and it is generally agreed that the
10 gravity-capillary wave energy is damped by a surfactant by the following mechanism. Immediately after a wave
11 field enters a surfactant patch, the Marangoni effect due to the viscoelastic film on the water surface increases
12 viscous dissipation of short wave energy at specific frequencies. This is caused by an additional dissipation in the
13 surface boundary layer. Indeed a shear stress in the boundary layer is required to balance the stress due to the
14 surface tension gradients originated by the non uniform concentration of the surface viscoelastic film (alternatively
15 contracted and expanded due to the passage of a wave). This gives rise to additional longitudinal waves in the
16 boundary layer superimposed on the existing surface waves that are thus damped by a resonance-type mechanism.
17 The dissipative spectral sink (the so-called Marangoni resonance region) is at frequencies between 3 Hz and 8 Hz,
18 the scale of the maximum damping depending on the dilatational modulus of the surfactant (Alpers and
19 Hühnerfuss, 1989; Fiscella et al., 1985). The resonant angular frequency ω_{res} for the Marangoni-force wave
20 damping is given by

$$\omega_{\text{res}} = \left\{ \frac{[\cos(\pi/8)]^4 g^4 (\eta \rho_w)}{\varepsilon^2} \right\}^{\frac{1}{5}} \text{ (rad/s)} \quad (1)$$

21 where g (m/s^2) is the gravity acceleration, ρ_w (kg/m^3) the clean water density, η (Ns/m^2) the clean water dynamic
22 viscosity, and ε (N/m) denotes the dilatational modulus of the surface film. As stated by Eq. (1), the larger the
23 modulus ε the longer the damped waves. The maximum damping of gravity-capillary waves is attained at a
24 frequency lower than ω_{res} (the Marangoni wave is a strongly damped wave) and the width of the resonant damping
25 is quite broad (the half-power width is in the order from 1 to 2 Hz; Alpers and Hühnerfuss, 1989).



1 In a more formal approach, the description of water surface gravity waves follows generally a statistical
 2 approach by means of the development of the wave elevation variance spectrum $E = E(k, \theta, \mathbf{x}, t)$ in the physical
 3 space \mathbf{x} and time t (k is the wavenumber and θ the propagation direction), its evolution governed by the energy
 4 balance equation (Gelci et al., 1957). In deep waters, it reads

$$\frac{\partial N}{\partial t} + \frac{\partial N}{\partial \mathbf{x}} \cdot (\dot{\mathbf{x}}N) = S_{\text{in}} + S_{\text{nl}} + S_{\text{di}} \quad (2)$$

5 where $N = E / \omega$ is the wave action density spectrum with ω the intrinsic angular frequency. Furthermore,
 6 $\dot{\mathbf{x}} = \mathbf{c}_g + \mathbf{U}$ with \mathbf{c}_g the wave group velocity and \mathbf{U} an appropriate current. The right hand side of Eq. (2)
 7 represents the net effect of sources and sinks for the spectrum (Komen et al., 1994): S_{in} is the rate of energy
 8 transferred from the wind to the wave field, S_{nl} is the rate of nonlinear energy transfer among wave components
 9 with different wavenumber, and $S_{\text{di}} = S_{\text{di,b}} + S_{\text{di,v}}$ is the rate of energy dissipation due to breaking ($S_{\text{di,b}}$) and viscous
 10 forces ($S_{\text{di,v}}$).

11 In our experiments the observations dealt with in this paper are the ones collected at steady state (we plan
 12 to deal with the transient in a different occasion), so that the spectrum at any fetch is determined by the upwind
 13 evolution of the source functions S_{in} , S_{nl} and S_{di} , that is

$$N = \int_0^x [(c_g + U)^{-1} (S_{\text{in}} + S_{\text{nl}} + S_{\text{di}})] dx \quad (3)$$

14 where, with good approximation, we have neglected the cross-tank wave energy evolution. The velocities \mathbf{c}_g and \mathbf{U}
 15 are also, but very weakly, fetch dependent. The balance in Eq. (3) indicates that any modification of the wave
 16 energy may and must be caused by changes in the rate of wind input, dissipation, or/and nonlinear transfer.

17 In presence of oil, all three source functions in Eq. (2) undergo a change compared to the clean water
 18 condition. Indeed, the rapid suppression of short waves by Marangoni forces reduces the water surface mean slope,
 19 which leads to a change of the wind vertical profile and rapid decrease of the momentum flux from the wind to the
 20 wave field (see, e.g., Mitsuyasu and Honda, 1986). Those two effects combined produce a change of the shape of
 21 the wave spectrum in the equilibrium range, which leads, via nonlinear wave-wave interaction (Hasselmann, 1962),
 22 to a slow leakage (but fast compared to the pure viscous one; Alpers and Hühnerfuss, 1989) at wavelengths longer
 23 than those at which the Marangoni forces are effective (Hühnerfuss et al., 1983 found that waves with wavelength
 24 around 3 m are significantly damped when they travel through a 1.5-km-long monomolecular surface film patch).



1 The result is that the wave field is rapidly smoothed and progressively attenuated as it propagates within a
2 surfactant patch (Ermakov et al., 1986).

3 Given the possible variability of the surfactant density on the water surface, it is natural to wonder about the
4 related sensitivity of the effect on waves. Analyzing the wind-wave tank experiments with surfactants (sodium
5 lauryl sulfate) presented by Mitsuyasu and Honda (1986), we can distinguish two different regimes for wave
6 attenuation, which correspond to weak and strong wave damping, respectively. Firstly, for small surfactant
7 concentrations (i.e. weak damping), the peak frequency of the wind-wave spectrum in presence of films is shifted
8 to higher frequencies in reference to the peak frequency of clean water (in other words waves develop more
9 slowly). However, spectra preserve u_* -similarity (u_* is the friction air velocity), and the new spectral shape was
10 ascribed mainly to the decrease of the wind stress: the surfactants smooth the surface and act reducing the wind
11 stress, therefore the waves grow less. We interpret this result assuming that for low surfactant concentrations the
12 effectiveness of the Marangoni damping is small (i.e. the water surface is not fully covered by an uniform film), but
13 with a partially reduced aerodynamic roughness. On the contrary, for the highest concentration (hence with a strong
14 damping) the similarity no longer holds, and most of the energy around the peak is lost (the maximum energy is at
15 a frequency smaller than the one in clean water; see also next Figure 5 and Figure 6).

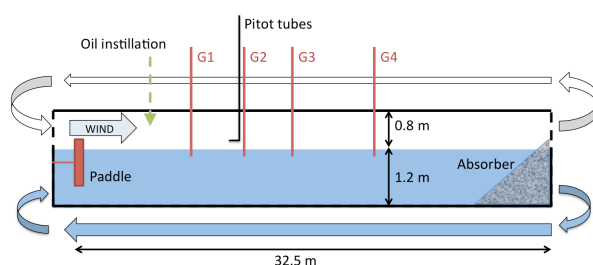
16 A question about Marangoni forces concerns the maximum wind speed for which they are expected to keep
17 their damping efficiency. In early studies, the disappearance of the Marangoni damping was observed by Mitsuyasu
18 and Honda (1986) for wind speed larger than a critical value, that those authors found to be 12.5 m/s. A possible
19 explanation is provided in the study by Alpers and Hühnerfuss (1989), who argued that above a certain friction
20 velocity (around 0.5 m/s) the Marangoni dip is filled in owing to a large flux of wave energy into the Marangoni
21 resonance region by nonlinear wave-wave interactions. In addition, for stronger wind stresses the viscoelastic film
22 becomes more mixed with the underlying clean water bulk (the film is “washed down”), so that the Marangoni
23 damping is strongly attenuated (see also Feindt, 1985). However, these conclusions seem not to be fully consistent
24 with the recent analysis made by Cox et al. (2017) of the saving in 1883 of the crew of a sinking vessel by the ship
25 *Martha Cobb* under very severe stormy conditions (wind speed around 20 m/s). In that occasion 19 liters of fish oil
26 were dribbled into the sea and the log records report what, after a 20-minute delay, was defined as a “magic effect”,
27 i.e. that the water surface smoothed and breakers disappeared around the vessel, allowing the crew to be saved
28 using a small open deck dingy. Cox et al. (2017) estimated that after 20 minutes the surface covered by the oil film



1 was about 0.4 km^2 , hence, the average oil thickness was about $5 \times 10^{-8} \text{ m}$. In those conditions, therefore, the
2 thickness was comparable to that used in the experiments in the tank and, in spite of the high wind speed, the wave
3 damping (with practical cancelling of wave breaking) was still effective.

4 2 Experimental facilities, experiments carried out, and data processing

5 The experiments described in this study were performed in a large wind- and paddle-wave facility allowing the
6 generation of winds at velocities comparable with those in open sea (but no extreme conditions). The
7 measurements were carried out in the flume of the First Institute of Oceanography (Qingdao, P.R. China) illustrated
8 schematically in Figure 1. The tank dimensions are: length 32.5 m , wall-to-wall cross-section 1.0 m , ceiling at 0.8 m
9 m above the mean water surface. The water depth is 1.2 m , satisfying the deep-water condition for the wind-driven
10 gravity-capillary, and practically also paddle, waves analyzed in this study. The smallest longitudinal natural
11 frequency of the tank is 0.052 Hz . Side walls are made of clear glass to enable visualization of the wave field. A
12 water pipe parallel to and below the flume allows the continuity between the two ends of the tank.



13

14 **Figure 1: Schematic longitudinal diagram of wave flume arrangement at the First Institute of Oceanography (FIO) flume (Qingdao,**
15 **P.R. China). For the sake of clarity, horizontal and vertical scales are distorted. The arrows indicate the direction of the flow.**

16 The wind tunnel is mounted atop the wave tank which is closed with side glass walls and ceiling. The
17 airflow could be driven up to reference speed of 12 m/s . Mechanically-generated (paddle) waves coexisting with
18 wind waves could be generated by a piston-type paddle in the range of periods from 0.5 s to 5.0 s (frequencies from
19 0.2 Hz to 2.0 Hz) and dissipated at the downwind end of the tank on a sloping beach of fibrous matter. Four
20 calibrated capacitance-type wave gauges collecting synchronous water surface elevation data for 300 s at 50 Hz
21 were distributed at fetches (along the tank main axis) $X = 8.0 \text{ m}$ (probe G1), 12.0 m (G2), 15.5 m (G3), and 20.5 m
22 (G4). The fetch $X = 0.0 \text{ m}$ corresponds to the inlet for wind in the water tank. For the statistically steady part of the



1 wave records the variance frequency-spectrum of water surface elevation $z(t)$ were computed by using the Welch's
2 overlapped segment averaging estimator (Welch, 1967).

3 For characterization of the airflow velocity vertical profile $U_a(h)$, five Pitot tubes sampling at 1 Hz have
4 been located at $X = 11.5$ m in the center of the cross-section and distributed at different heights h above the still
5 water surface, respectively (from tube 1 to 5) at $h = 8.3$ cm, 18.3 cm, 28.3 cm, 38.3 cm, and 48.3 cm. Estimates of
6 the wind stress was derived from air velocity average profiles using Pitot tube observations fitted with a
7 logarithmic profile. The accuracy of the wind stress obtained from the profiles measured by Pitot tubes in a wave
8 tank was examined by Liberzon and Shemer (2011) who found that the values of the wind stress obtained from the
9 measurements by the Pitot tube and those calculated from the Reynolds stresses (using a X-hot-film thermo-
10 anemometer) agree within about 10 % mean difference.

11 Our experiments aimed at analyzing the different results, using the different combinations of reference
12 wind speed U_r , paddle waves (changing the peak wave period T_p , and significant wave height H_s) and oily surface.
13 The data of each experiment were later screened for correct data availability and consistency among the different
14 instruments. This led to exclude several records considered not suitable (independently of the physical results) for
15 the final analysis. This was based on the six experiments listed in Table 1. Two different blower reference speeds
16 were analyzed, namely $U_r = 6$ m/s and 8 m/s, and one set of irregular paddle waves (JONSWAP spectrum with $T_p =$
17 1.0 s and $H_s = 6.2$ cm; steepness $H_s / L_p = 0.04$, with L_p the peak wavelength). Note that many of these experiments
18 have been repeated up to four times. All experiments were initiated with no wind and undisturbed water surface.

Exp.	W06	W06-O	W06-O-NI	W08	W08-P	W08-P-O
Wind	6 m/s	6 m/s	6 m/s	8 m/s	8 m/s	8 m/s
Paddle	-	-	-	-	JONSWAP Spectrum ($T_p = 1.0$ s, $H_s = 6.2$ cm)	JONSWAP Spectrum ($T_p = 1.0$ s, $H_s = 6.2$ cm)
Oil	-	Instillation	No instillation	-	-	Instillation

19 **Table 1: List of experiments performed in the wind- and paddle-wave tank, using clean water (ordinary tap water) and after**
20 **instilling fish oil. The wind speed is the reference value U_r imposed at the blower. For paddle waves, T_p is the peak period and H_s the**
21 **significant wave height. Blanks denote not applicable cases.**

22 Three experiments (two with wind waves and one with wind and paddle waves) were made with the fish
23 oil-covered water surface. The dilational modulus ε of this type of oil is roughly 0.03 N/m (Foda and Cox, 1980),
24 hence its resonance frequency is estimated to be $\omega_{res} = 23.7$ rad/s (i.e. linear frequency of 3.77 Hz and wavelength



1 of about 11 cm). Moreover, the radial spreading speed of fish oil is around 0.14 m/s, sufficiently large to keep
 2 uniform the oil film that might be broken by the wave action (Cox et al., 2017). Before performing the experiments
 3 with the slick-covered surface, the oil was instilled from the ceiling at fetch $X = 4$ m, releasing 26 drops with the
 4 blower at rest. Estimating each drop of volume about $50 \times 10^{-9} \text{ m}^3$, the average oil thickness on the water surface
 5 was 4×10^{-8} m, namely few molecular layers. During the experiments W06-O and W08-P-O (see Table 1) the oil
 6 film was preserved (see later in section 3.1) by continuously instilling onto the water surface oil drops, while the
 7 dropping was interrupted (no instillation) at the onset of the wind start of the experiment W06-O-NI.

8 A crucial point in wind wave tank measurements concerns the correct reference system for waves generated by
 9 wind. The wave data acquired by the probes in the tank are represented in a fixed (absolute) reference system,
 10 while the response of the wave field to the oil film is intrinsic in the wave dynamics. Therefore the sea surface
 11 elevation energy spectrum E must be mapped in a reference system moving with the wind-generated near-surface
 12 water current. To this end, the wave spectrum must therefore be transformed from absolute f_a to intrinsic
 13 frequencies f_i , i.e. those that would have been recorded by a probe moving with the current. Indeed, for waves
 14 propagating over a moving medium, the Doppler effect modifies the observed frequency of each elementary
 15 periodic wave that makes up the random wind field (Lindgren et al., 1999). This effect can be particularly large for
 16 short waves at sea (modifying the slope of the high-frequency spectrum tail; Benetazzo et al., 2018) and in a wave
 17 tank where waves are generally short whilst the current speed can be a non-negligible fraction of the wave phase
 18 speed.

19 For harmonic waves in the limit of small wave steepness and neglecting the modulation of short waves by long
 20 waves (Longuet-Higgins and Stewart, 1960), the relation between f_a and f_i is given by (Stewart and Joy, 1974):

$$f_a - f_i - [ku_w \cos(\theta - \theta_U)] / (2\pi) = 0 \quad (4)$$

21 where u_w is an appropriate (Kirby and Chen, 1989; Stewart and Joy, 1974) water velocity vector (of direction θ_U),
 22 and θ the wave direction. At the leading order, it is assumed that the dispersion relationship of the gravity-capillary
 23 wave theory provides a unique relationship between the frequency f_i and the wavenumber k as follows:

$$2\pi f_i = \sqrt{gk + \frac{T}{\rho} k^3} \quad (5)$$

24 with T the water surface tension, ρ the water density, and g is the gravity acceleration. In accordance to Eq. (4),
 25 the spectral representation in absolute frequencies experiences a shifting of the energy distribution (see Figure 5



1 below). In our case, we assume that short waves in the tank mostly feel the surface current drift and we neglect the
2 Doppler shift associated with the orbital motion of long waves. That drift can be estimated by the wind speed (see
3 later), and reasonably assumed aligned with the waves (namely, $\theta = \theta_U$). Hence, the frequency spectrum in intrinsic
4 coordinates may be derived as

$$E(f_i) = E(f_a) J_{ai} \quad (6)$$

5 where $J_{ai} = |df_a / df_i|$ is the Jacobian of the transformation, which in the limit of deep water can be written explicitly
6 as

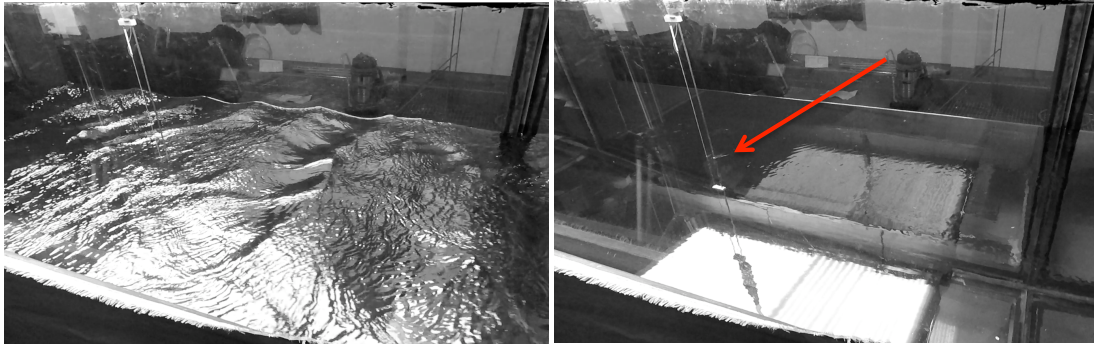
$$J_{ai} = |1 + 2u_w \sqrt{gk + \frac{T}{\rho} k^3} / (g + 3\frac{T}{\rho} k^2)| \quad (7)$$

7 **3 The basic results**

8 We analyse and discuss in sequence the results of each set of experiments. We draw progressively our conclusions,
9 each one to be then possibly utilised for the analysis of the later sets.

3.1 Wind waves without and with oil

10 We begin the examination of the change of gravity-capillary wave properties caused by the fish oil film by
11 analyzing the effects on the water elevation z and wind speed profile $U_a(h)$ during the experiments W06 ($U_r = 6$ m/s
12 and clean water) and W06-O (the same as W06, but with oil slick). For the latter, the wind wave field attenuation
13 due to the Marangoni forces is readily visible in Figure 2 that shows two pictures of the water surface (taken nearby
14 the fetch of 20 m) without (left panel) and with (right panel) the oil instillation. After the oil film is spread on the
15 water, the surface is largely smooth, with only tiny elevation oscillations (1 mm at most; see Figure 4) and there
16 appear to be no organized wave motion (see also the videos available as supplementary material SM1). The
17 presence of an extremely thin (practically mono-molecular) layer of oil on the surface alters heavily the air-sea
18 interface properties. It is instructive to analyze the situation first from the air, then from the water, point of view.



1

2 **Figure 2:** Two photographs showing the water surface condition at fetch of about 20 m taken without (left panel) and with oil
 3 instillation (right panel). On both cases the water surface was forced with a reference wind speed $U_r = 6$ m/s (blowing from left to
 4 right on the pictures). The wave probe G4 is visible on the left-hand side of both pictures. The red arrow in the right panel points to
 5 the oscillating flow (vortex shedding) past the probe. See also the video available as supplementary material SM1.

6 **3.1.1 Airflow characterization**

7 We begin evaluating the air-side stress due to the wind drag on the water surface. In this respect, the wind speed
 8 vertical profile above the water surface was approximated using the Pitot tube records of the along-channel air
 9 speed profile, namely $U_a(h)$. For an aerodynamically rough airflow, the along-channel component of the mean wind
 10 speed \bar{U} in the outer turbulent layer at height h above the boundary is expected to follow a self-similar Karman-
 11 Prandtl logarithmic law as a function of height

$$\bar{U}(h) = \frac{u_*}{\kappa} \log\left(\frac{h}{h_0}\right) \quad (8)$$

12 where the overbar indicates the temporal averaging process, u_* is the friction velocity along the same direction as
 13 \bar{U} , $\kappa = 0.41$ is the von Kármán's constant. The non-zero parameter h_0 has the meaning of the roughness height
 14 where \bar{U} appears to go to zero (namely h_0 is the virtual origin of the mean velocity profile). In presence of waves,
 15 the shape of the wind velocity profile $\bar{U}(h)$ is governed by both turbulent and wave-induced momentum flux, the
 16 latter being function of the source term S_{in} (the transport of horizontal momentum due to molecular viscosity is
 17 considered negligible, except very near the surface where the vertical motion is suppressed). The total air-side
 18 shear stress τ_a at the boundary of the flow is then approximated as

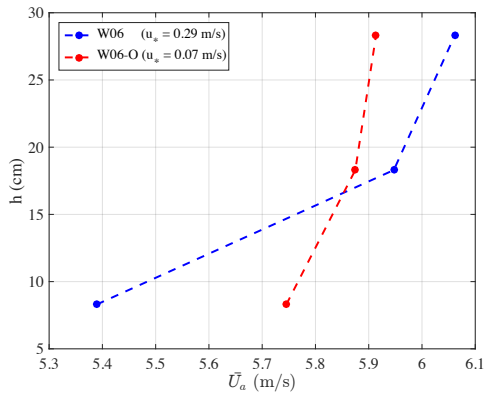
$$\tau_a = \rho_a u_*^2 \quad (9)$$

19 with ρ_a the air density.



1 To account in Eq. (8) for the non-slip condition, the measured airflow velocity $U_a(h)$ has to be taken relative
2 to along-wind components of the water velocity u_{w0} at $h = 0$, namely $U(h) = U_a(h) - u_{w0}$. It is thus assumed that the
3 mean water surface drift velocity u_{w0} constitutes the boundary condition at $h = 0$ for the vertical profile of the
4 airflow velocity. Wu (1975) found that at the air-water interface, the wind-induced current is proportional to the
5 friction velocity of the wind, and it results from the wind shear, Stokes drift, and momentum injection during wave
6 breaking events. For non-breaking wavy surfaces, the wind-induced surface current was determined to be around
7 50% of the airflow friction velocity (Phillips and Banner, 1974 and Wu, 1975). In a (clean water) wind-wave tank
8 and at steady conditions the value of u_{w0} can be related to the maximum value of $U_a(h)$ which is not achieved at the
9 largest distances from the water due to the presence of the tank roof. A value u_{w0} around 3.3% of the free-stream
10 maximum wind velocity seems to be a reasonable approximation (Liberzon and Shemer, 2011; Peirson, 1997; Wu,
11 1975) and was used in this study.

12 In the experiment W06 the maximum value of $\bar{U}_a(h)$ of 6.06 m/s was found, attained at the third Pitot tube,
13 namely at $h = 28.3$ cm from the still water surface. Hence, accounting for a surface water speed $u_{w0} = 6.06 \times 0.033 \approx$
14 0.2 m/s, a logarithmic curve was fitted (the mean absolute error of the fitting is 0.01 m/s) to the average profile
15 $\bar{U}(h)$ shown in Figure 3 and the two parameters $u_* = 0.29$ m/s and $h_0 = 0.1$ mm were estimated. For the lowest
16 Pitot tube ($h = 8.3$ cm), the dimensionless height $h_* = gh/u_*^2$ is 9.7, implying that up from there wind data were
17 collected in a region where turbulent stresses are expected to dominate over wave-induced stresses (Janssen and
18 Bidlot, 2018). The typical viscous sublayer thickness approximated as $11.6\nu/u_*$ measured 0.04 mm, such that the
19 atmospheric boundary layer appears to be aerodynamically rough. The wind shear stress τ_a based on the
20 measurement in this layer equals 0.10 N/m². The equivalent wind speed at height $h = 10$ m, extrapolated from Eq. (
21 8), is $\bar{U}_{10} = 8.6$ m/s, which is in satisfactory agreement with the typical relation between u_* and \bar{U}_{10} found in a
22 wind-wave tank filled with clean water (Mitsuyasu and Honda, 1986). The neutral drag coefficient measured at 10
23 m height and defined as $C_D = (u_*/\bar{U}_{10})^2$ is 1.1×10^{-3} . The values of u_* and h_0 are in agreement with those obtained
24 in the experimental results of Liberzon and Shemer (2011), and those estimated by the bulk parameterization of
25 air-sea turbulent fluxes provided by the Coupled Ocean-Atmosphere Response Experiment (COARE) algorithm
26 (Fairall et al., 2003) that gives $\tau_a = 0.11$ N/m², using as input the profile $\bar{U}(h)$ determined in our experiments.



1

2 **Figure 3: Vertical profile of the mean horizontal wind speed \bar{U}_a measured over the water surface at fetch $X = 11.5$ m. Reference wind**
 3 **speed $U_r = 6$ m/s. Clean water conditions (blue) and oil-covered surface (red). In the legend, the value of the airflow friction velocity**
 4 **u_* is shown within brackets. Only the value recorded at the three lowest Pitot tubes are shown.**

5 The smoothing of the water surface in presence of oil reflects on the airflow, which differs from that over
 6 clean water and has a smaller vertical gradient $d\bar{U}_a/dh$ of the wind speed (Figure 3). Because of the reduction of
 7 the resistance on the water surface, the wind speed strengthens over the film-covered surface, but the effect is
 8 limited to the lowest part of the turbulent airflow. Similar behavior was observed in the wind-wave tank
 9 experiments by Mitsuyasu and Honda (1986). For continuity reasons, i.e. for the (practically) constant airflow
 10 discharge in the tank (the difference of the discharges measured by the Pitot tubes is smaller than 1%), a less steep
 11 wind profile implies a lower velocity (with respect to the clean water case) in the central line of the flow (with oil
 12 the maximum value of $\bar{U}_a(h)$ was 5.91 m/s).

13 In the case of the oil film-covered surface, a problem arises, i.e. if the 3.3%-rule still holds to determine the
 14 surface current drift from the wind speed. The problem stems from the fact that for clean surfaces the momentum
 15 flux to the water column (i.e. for the generation of current) is the sum of the flux transferred across the air-sea
 16 interface not used to generate waves and the momentum flux transferred by wave breaking. In terms of spectral
 17 quantities the stress to the water column τ_w can be computed as

$$\tau_w = \tau_a - \rho_w g \int_0^{2\pi} \int_0^{k_{\max}} \frac{k}{\omega} (S_{\text{in}} + S_{\text{nl}} + S_{\text{di}}) dk d\theta \quad (10)$$

18 where we have omitted the direction of the flux that we assume aligned with the flume main axis. In the high-
 19 frequency equilibrium range, the momentum coming from the wind is dissipated, and is therefore directly
 20 transferred to the water column.



1 The balance in Eq. (10) is plainly altered for the oil-covered surface analyzed in this study, as it is visible
2 in the right panel of Figure 2, for which we assume $S_{in}+S_{nl}+S_{di} = 0$. In this case, the wave-induced transport
3 becomes negligible and hence the total current drift is supported only by the stress exerted τ_a by the wind at the air-
4 sea interface. In this respect, from visual inspection of the supporting movies acquired during the experiments (see
5 the video available as supplementary material SM1), we did observe the presence of a water surface drift and a
6 high-frequency oscillating flow (vortex shedding) downstream from the probes' beams (the shedding at G4 is
7 pointed by the red arrow in the right panel of Figure 2). The latter implies the presence of a near-surface drift
8 impacting the probes. No adequate instrumentation (e.g. Particle Image Velocimetry; see e.g. Adrian, 1991) had
9 been designed in advance to obtain a representation of the fluid flow close to the wavy air-water interface.

10 However, the availability of video-camera images allowed two independent estimates of near-surface water
11 drift. The first one was possible tracking the motion of tiny bubbles moving on the water surface along the tank and
12 clearly visible in the 1920x1080 pixel images captured at 60 Hz by a video-camera placed outside the tank, close to
13 the probe G4. A detailed description of the procedure is given in Appendix A. The distribution of the so-defined
14 surface speed has mean value of 26 cm/s and standard deviation of 11 cm/s. Albeit the relatively large variability,
15 such observations clearly show that, even if the stress on the water surface is largely reduced by the oil film, a
16 surface current is still present whose order of magnitude is comparable with what one expects in clean water. A
17 possible objection to this approach is that the bubble motion could be due, partly at least, to the wind drag.
18 However, this estimate, albeit with some approximation, is supported by the second indirect estimate. On the right
19 panel of Figure 2 the wave probe across the surface is clearly visible, and there a “wake” behind it. Indeed, as we
20 will soon discuss, the wave spectra show an isolated peak around 10 Hz that we interpret as due to the vortex
21 shedding caused by the surface current flowing around the probe support (diameter $d = 4$ mm). Use of the related
22 vortex shedding frequency $f \approx 0.21u_{w0,oil} / d$ (see later in subsection 3.1.2) suggests $u_{w0,oil} = 20$ cm/s that is close
23 (actually less than) the estimate using bubbles (which probably were partially also drifted by wind).

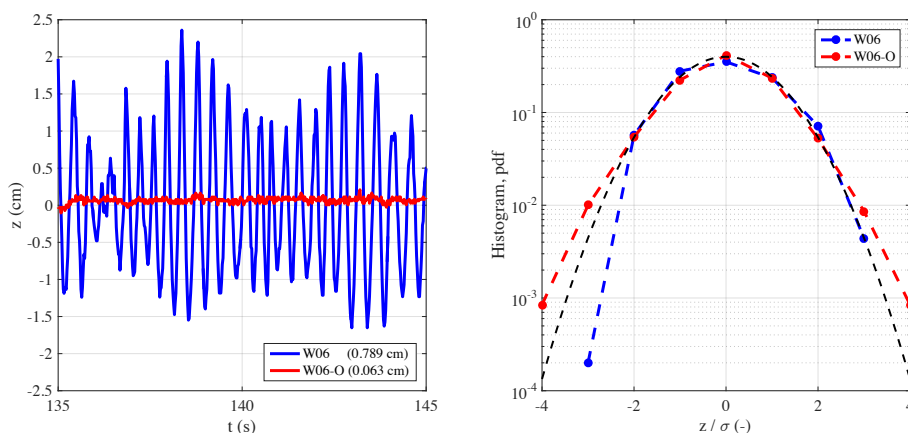
24 With this information, we have found that the wind stress for oil-covered smooth surface is $\tau_{a,oil} = 0.005$
25 N/m^2 , approximately 5% of τ_a , and the drag coefficient undergoes a decrease of one order of magnitude. The
26 extrapolated 10-m height wind speed $\bar{U}_{10,oil}$ is 6.3 m/s, smaller than \bar{U}_{10} , in contrast to the field observations of
27 Ermakov et al. (1986), most likely because our observations were collected in a tank with an upper roof. The
28 roughness height was determined to be very close to zero, implying that the air boundary layer for the oil-covered



1 water shows properties of a hydrodynamically smooth flow. This conclusion supports the idea presented in
 2 Mitsuyasu and Honda (1986) and discussed by Mitsuyasu (2015), who showed also that for low wind speeds (few
 3 meters per second) the water surface properties are similar in clean water and in water with oil.

4 3.1.2 Wave field characterization

5 In presence of the viscoelastic oily film, the gravity-capillary wave damping is quantified by analyzing the time
 6 records $z(t)$ of the sea surface elevation field at different fetches. In this respect, Figure 4 (left panel) gives a clear
 7 idea of the Marangoni damping effect, which can be quantified by noting that the standard deviation σ of $z(t)$
 8 shrinks by one order of magnitude. However, the process does not involve only a decrease of the vertical
 9 oscillations, as it is the whole spatio-temporal distribution of the surface elevations that is abruptly changed (right
 10 panel of Figure 4). Indeed, whereas in clean water, in active wave generation, the histogram of z (high-pass filtered
 11 above 1 Hz; see discussion below) has a positive skewness coefficient (as it is expected for wind-waves; see
 12 Longuet-Higgins, 1963), in presence of oil the empirical histogram is quasi-symmetric around the mean (the
 13 skewness coefficient is -0.03, very close to zero). This implies that for slick-covered surfaces the generation and
 14 evolution of gravity-capillary waves are governed by different balance and process, which are dominated by the
 15 reduced wind input and the Marangoni energy sink, which lead to a quasi-Gaussian surface elevation field at all
 16 scales.

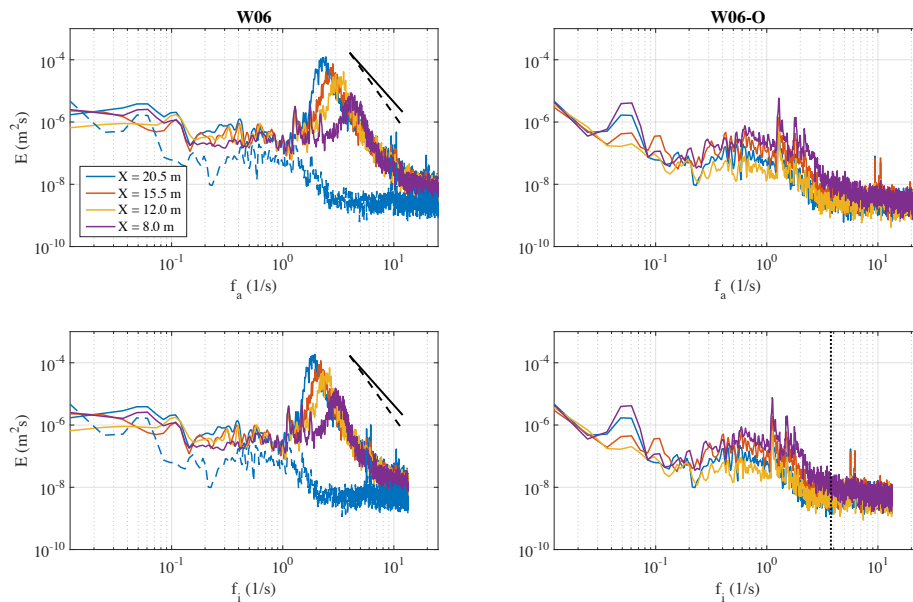


17

18 **Figure 4:** Sea surface elevation for clean (blue) and slick-covered (red) surface. (left) Extract of the single-point record $z(t)$ at $X =$
 19 **20.5 m** (probe G4) for the two conditions with clean water (experiment W06) and after the oil instillation (W06-O). In the legend, the
 20 value of the standard deviation σ of $z(t)$ is shown within brackets. (right) Histogram of the normalized elevations, high-pass filtered
 21 above 1 Hz (see discussion below). The black dashed line shows the Gaussian probability density function (pdf).



1 The most general and quantified view of the effect of oil is provided by the spectra $E(f_a)$ and $E(f_i)$
 2 (respectively absolute and intrinsic frequency) of water elevations. These are shown in Figure 5, for experiments
 3 W06 (left panel) and W06-O (right panel). For a more direct comparison the G4 oil spectrum is reproduced in the
 4 no-oil diagram (dashed blue line). The spectrum $E(f_i)$ was computed using the Jacobian transformation described in
 5 section 2 and assuming all wavenumbers as shifted by the same current equal to that on the surface, namely $u_{w0} =$
 6 0.2 m/s. Note in the “intrinsic” spectrum the expected shift towards lower frequencies, more evident in the right
 7 side of the spectrum where higher frequencies move with a lower speed with respect to the current. As physically
 8 sound, from now on all our considerations will deal with the intrinsic-frequency quantities. Starting with clean
 9 water conditions (left panels), the variation of the wave spectra with fetch is characterized by the expected
 10 downshift and overshoot of the peak of the spectrum. The total wave energy increases with fetch: the significant
 11 wave height H_s grows from 1.21 cm at the shortest ($X = 8$ m) fetch to 3.16 cm at $X = 20.5$ m. It is remarkable that
 12 for the slick-covered surface, there is no evidence of wave growth with fetch (right panels).



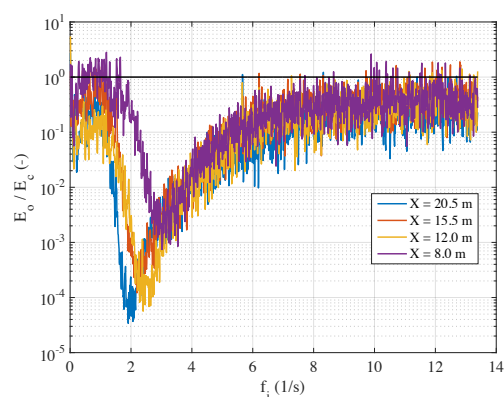
13

14 **Figure 5: Wave energy spectra $E(f_a)$ and $E(f_i)$ of the water surface elevation $z(t)$ at different fetches. Reference wind speed $U_r = 6$ m/s.**
 15 **(left) Clean water experiment W06. (right) Water with oil experiment W06-O (the spectrum at the fetch $X = 20.5$ m is replicated with**
 16 **a blue dashed line on the left panels). The black solid and dashed lines are the reference spectral shape proportional to f^{-4} and f^{-5} ,**
 17 **respectively. The vertical gray dotted line on the bottom-right panel shows the fish oil resonance frequency $f_{res} = \omega_{res}/(2\pi) = 3.77$ Hz.**



1 Focusing for the time being on the comparison among the oil and no-oil cases, the differences are obviously
2 macroscopic, but it is worthwhile to analyse them for different frequency ranges. For low frequencies, say below 1
3 Hz, there is clearly some energy also in the oily spectra. Note the peaks (around 0.05 Hz) at the G1 and G4 spectra,
4 reduced at G2 and G3. Remembering (see section 2) the longitudinal natural frequency of the tank, we interpret
5 these as “seiches” of the wave tank, obviously more visible the further the gauges are from the center of the tank. In
6 the clean water case more distributed oscillations exist, that we associate to a more active action of a possibly
7 irregular wind flow. The most interesting range is of course between 1 Hz and 4 Hz (close to the fish oil resonance
8 frequency). Here the effect of oil is macroscopic, with oil-case energy several orders of magnitude smaller than
9 without oil. Finally, still for the oil spectra, no wave signal is visible above 3-4 Hz where we should expect the
10 maximum damping of surface waves due to the oily surfactants (Alpers and Hühnerfuss, 1989).

11 A more direct comparison between the W06 and W06-O spectra is obtained showing in Figure 6 for each
12 frequency the ratio of the respective spectral energies. If we represent the frequency/fetch-dependent damping
13 coefficient as the ratio $D(f_i, X) = E_o / E_c$ between the variance density spectrum of the water surface elevation with
14 oil slick (E_o) and in clean water (E_c), we then find D values as small as 10^{-4} at the longer fetches. Of course the
15 maximum differences are at the peak frequency of the no-oil spectra, the respective frequency and ratio decreasing
16 with fetch while the no-oil energy increases.



17
18 **Figure 6: Damping of the wave energy for oil-covered water surface. The damping coefficient is evaluated as the ratio $D = E_o / E_c$**
19 **between the variance density spectrum of the water surface elevation with oil slick (E_o) and in clean water (E_c). The solid black line**
20 **shows the level $E_o = E_c$.**

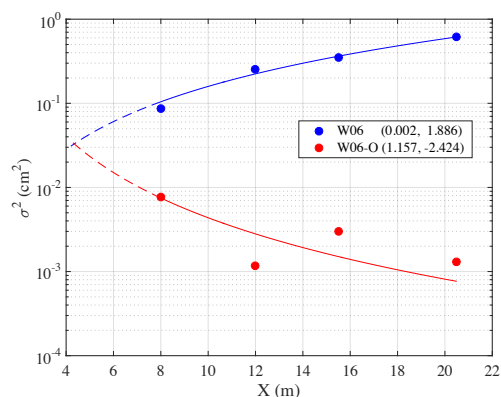
21 For a non-trivial detail of how to interpret the data from the experiments it is instructive to plot how energy
22 depends on fetch. In Figure 7 we show how the corresponding surface elevation (high-pass filtered above 1 Hz)



1 variance $\sigma^2 = \langle (z(t) - \langle z(t) \rangle)^2 \rangle$ (the angle brackets $\langle \rangle$ denote the ensemble average) varies for the clean water
 2 and oil cases. Granted the different orders of magnitude, it is macroscopic that, while the clean water wave energy
 3 grows with fetch, the opposite is true (or is suggested to be) with oil. To quantify better the fetch dependence we
 4 have fitted a power law

$$\sigma^2 = \alpha X^\beta \quad (11)$$

5 to the water surface variance σ^2 versus fetch X . The values of α and β , respectively, are tabulated in the legend of
 6 Figure 7 (with σ^2 in cm^2 and X in m).



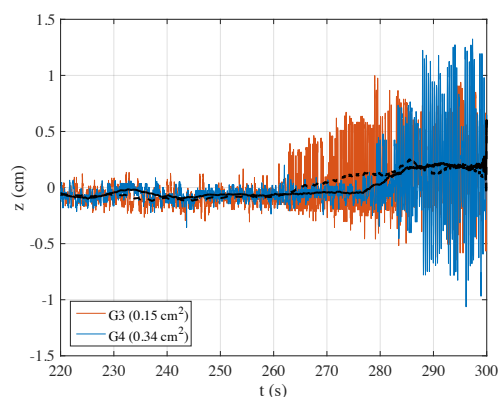
7
 8 **Figure 7: Spatial evolution of the water surface elevation variance σ^2 in clean water (W06) and with fish oil slick (W06-O). The solid**
 9 **lines are the power law-type function $\sigma^2 = \alpha X^\beta$ fitting the observations (in the legend, the coefficient α and β , respectively, are**
 10 **tabulated), while the dashed lines show the law extended outside the observed data interval.**

11 Prolonged backwards out of the experimental range in the figure, the two fitted laws intersect each other
 12 around $X = 4$ m. This suggests an explanation. This is the fetch at which oil was introduced into the tank. Note that
 13 in the W06-O experiment oil was continuously instilled during the experiment. This was because the wind, acting
 14 on the surface oil and creating, as we have seen, a current, tends to push it along the tank faster than the oil tends to
 15 distribute uniformly on the surface (with radial speed around 14 cm/s). Indeed this was smaller than the speed of
 16 the oily water surface we have discussed and derived in the previous sub-section discussing the airflow
 17 characterization. While the continuous, although very limited, instillation of oil during W06-O ensured the
 18 presence of oil film from the instillation point onwards, the wind, acting from fetch $X = 0$ m, was pushing the oil
 19 away from the first four-metre zone where therefore waves could be generated, hence equal, in both the oil and the
 20 no-oil cases. Therefore the “oil” energy we see in Figure 7 at eight-metre fetch is the remnant of the one previously



1 generated and already partially dissipated (between the 4 and 8 m fetches) due to the acting Marangoni forces.
 2 Incidentally, this explains one point we had deliberately avoided while discussing the spectra in Figure 5, i.e. why
 3 the highest energy in the oily spectra (right panel) is in the first spectrum, i.e. the shortest fetch.

4 The shift along the tank of the surface oil film is well illustrated by the results of the experiment W06-O-
 5 NI, i.e. when, starting with a layer of oil well distributed on the water surface in the tank, we did not further
 6 instillate oil during the action of the wind (reference wind speed $U_r = 6$ m/s). The resulting records at $X = 15.5$ m
 7 (G3) and 20.5 m (G4) are shown in Figure 8. It is obvious that around 262 sec the effect of oil is beginning to
 8 vanish at G3, followed 15-20 s later by a similar result at G4. Note that this does not mean the whole oil was
 9 pushed past G3 at 262 sec. Were this the case we should see in the record the already (up to G3 position) generated
 10 waves. Rather, the oil edge is getting close enough to let G3 feel the consequences, which are different from those
 11 at G4: in the range [290 s, 300 s] H_s grows from 1.56 cm (G3) to 2.34 cm (G4), conveying the fact that a longer
 12 fetch was progressively made clean by the near-surface water drift. The progressively increasing space free of oil is
 13 also manifest in the record of each probe, where the basic wave period tends to increase with time.



14

15 **Figure 8: Sea surface elevation at probes G3 ($X = 15.5$ m) and G4 ($X = 20.5$ m) for an initially slick-covered surface without oil**
 16 **instillation (experiment W06-O-NI). The dashed and solid black lines show the smoothed elevations (moving average of size 5 s) at**
 17 **G3 and G4, respectively. In the legend, the variance of $z(t)$ within the range of $290 \text{ s} \leq t \leq 300 \text{ s}$ is reported.**

18 In the experiment W06, spectra at the longer fetches (probes G3 and G4, see Figure 5) show two highly
 19 energetic and very close peaks around the frequency $f_a \approx 10$ Hz. As mentioned in section 3.1.1, our interpretation is
 20 that they are originated by the vortex-induced vibrations at the cylindrical holding beams of the probes. Indeed, the
 21 frequency f_v at which vortex shedding takes place is related to the Strouhal number by the following equation:

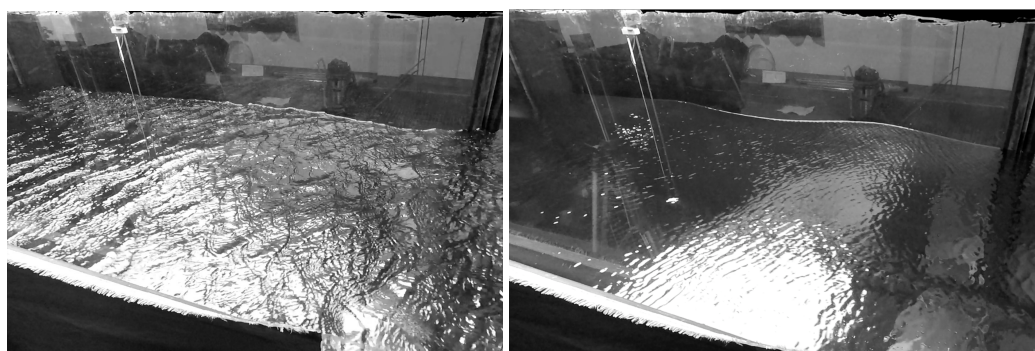


$$St = \frac{f_v d}{u} \quad (12)$$

1 where St is the dimensionless Strouhal number, f_v is the vortex shedding frequency, d is the diameter of the body,
2 and u is the flow velocity. The Strouhal number depends on the Reynolds number, but a value of 0.21 is commonly
3 adopted (Steinman, 1946). Adopting $d = 0.4$ cm (the diameter of the probe's holding beam) and $u = 20$ cm/s, the
4 vortex frequency is $f_v = 10.5$ Hz, consistent with the experimental evidence. Elaborating this point further, it is
5 worth noting that similar spectral peaks (as energy and frequency) have been found also during the W06-O
6 experiment. In our interpretation, this evidence supports the fact that the water surface drift was generated by the
7 wind friction also in presence of oil, and that its magnitude is consistent with the one expected in clean water
8 conditions.

3.2 Wind and paddle waves without and with oil

9 The second series of experiments was done adding mechanically-generated paddle waves to the wind-generated
10 ones, both in clean water and in water with fish oil. Within the general purpose of a better understanding of the
11 related air-sea interactions, we had two specific purposes. The first one was to explore the influence of pre-existing
12 relatively long waves (the paddle generated ones) on the local generation of wind waves. The second purpose was
13 how this interference was modified by the presence of fish oil. These second set of experiments (namely W08-P
14 and W08-P-O) was done with 8 m/s nominal wind speed. Of course a 6 m/s value would have allowed a more
15 direct comparison with the results obtained without paddle waves (previous section). At the same time, a higher
16 wind speed was useful to better highlight the interaction with the paddle waves. Originally we had planned two full
17 sets of parallel experiments. However, as mentioned in section 2, the strict condition of analyzing only good quality
18 data left us with what is listed in Table 1. As we have seen and will see, the available data suffice for providing a
19 number of remarkable results.

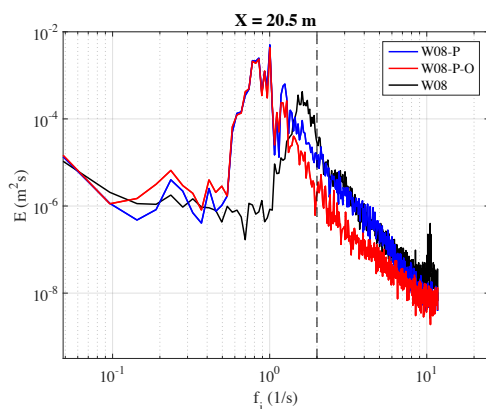


1

2 **Figure 9: Two photographs of the water surface condition at fetch of about 20 m taken without (left panel, experiment W08-P) and**
3 **with oil instillation (right panel, experiment W08-P-O) onto wind-waves (wind blowing from left to right of the pictures at the**
4 **reference wind speed $U_r = 8$ m/s) and irregular paddle-waves. See also the videos available as supplementary material SM2.**

5 In the tank paddle waves were nominally generated as a JONSWAP-like spectrum with 6.2 cm significant
6 wave height and 1.0 sec peak period. On top of this wind waves were generated (within limits) by a reference 8 m/s
7 wind (experiment W08-P). The resulting situation is shown in (Figure 9, left panel), the picture being taken, as
8 Figure 2, close to fetch $X = 20.5$ m. Starting with a qualitative perception from the image (see also the videos
9 available as supplementary material SM2), we derive, as expected from what is reported in the literature, that wind
10 waves grow substantially less than expected in a pure wind sea. Incidentally, for a full comparison we also ran the
11 W08 experiment ($U_r = 8$ m/s without paddle waves in clean water). We will soon show also this result. The
12 comparison between Figure 2 and Figure 9 is even more striking considering the larger speed in Figure 9. Clearly
13 the presence of the paddle waves has an effect. This is a matter of practical relevance for the cases when in the
14 ocean fresh new waves are generated superimposed on a pre-existing swell (in this case propagating along the same
15 direction). A more quantified comparison of W08-P versus W08 (i.e. with versus without paddle) is provided by
16 the wave spectra shown in Figure 10. Ignoring for the time being the oily results (experiment W08-P-O), we see
17 that the introduction of the paddle waves (with a JONSWAP spectrum) cancels the wind wave peak of W08 at
18 about 1.6 Hz. However, the tails of the two spectra somehow converge above 2.2 Hz. As we will soon see, with
19 paddle waves the conditions did not allow the visual measurement of current.

20



1

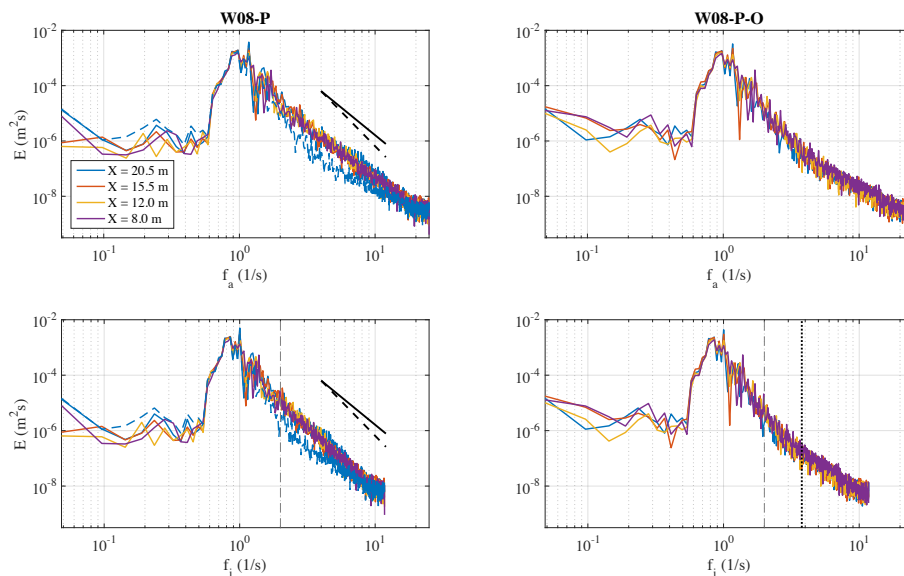
2 **Figure 10: Variance density spectrum $E(f)$ of the water surface elevation $z(t)$ at fetch $X = 20.5$ m (wave probe G4) in presence of co-**
3 **existing wind and paddle waves in clean water (W08-P), wind and paddle waves in water with oil (W08-P-O), and wind waves only in**
4 **clean water (W08). The dashed gray vertical line shows the maximum frequency (2 Hz) produced by the paddle.**

5 In the open ocean, the influence of swell on local wind wave generation is a known fact. Hwang et al.
6 (2011) discuss how the Tehuano-wind generated waves, on the Pacific coast of Mexico, are affected by the
7 incoming oceanic opposing swell. With some similarity, the cases of following or opposing swell seem to differ
8 somehow in their physics. The “following swell” case was first studied by Mitsuyasu (1966) and later intensively
9 by Donelan (1987) who suggested that a swell (in practice paddle waves; also his experiments were done in a wind-
10 and paddle-wave tank at the University of Miami, USA) induces a detuning of the resonance conditions for non-
11 linear interactions among wind waves. Later, in the studies by Phillips and Banner (1974) and Donelan et al. (2010)
12 the suggested explanation was the enhanced wind wave breaking due to the wind and paddle waves interactions.
13 Also, the influence of paddle waves increases with their steepness. More recently, Chen and Belcher (2000)
14 proposed the idea that the long wave exerts a drag on the airflow, which reduces the turbulent stress in the airflow
15 that is available to generate wind waves.

16 It is instructive to see how the overall effect (both without and with oil) varies with fetch. The related
17 spectra are in depicted in Figure 11. Contrarily to the pure windy cases (experiments W06 and W08), there appear
18 to be no evident dependence on fetch of the wave energy. Our interpretation is the following. On the one hand the
19 disappearance of the wind sea energy peak in presence of long waves implies that wind wave peak does not
20 develop with fetch. On the other hand, in water with oil, at higher frequencies the balance is between non-linear
21 interactions and Marangoni dissipation, which is only slightly depending on fetch. Note that, as clearly represented

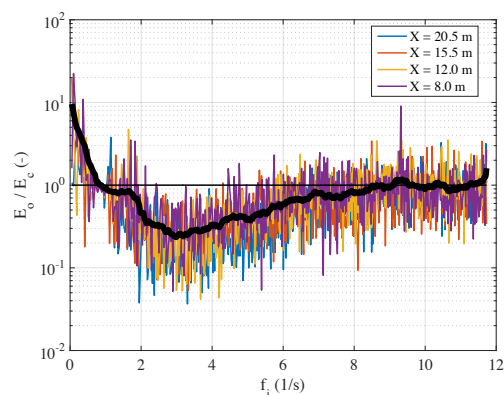


1 in Figure 12, the attenuation is maximum around 3 Hz (smaller than the resonance frequency) and the maximum
 2 damping of wind wave energy (see for comparison Figure 6) is such that the level of damping (D) is two and three
 3 orders of magnitude smaller than with only wind waves (experiments W06). This is the consequence of two
 4 parallel facts: less wind wave energy in presence of paddle waves, and a decreased efficiency of damping by oil
 5 film (as evident comparing the right panels of Figure 2 and Figure 9). One explanation for this latter effect is that
 6 the stretching, due to swell, of the thin (almost) mono-molecular layer of oil breaks its continuity, hence decreasing
 7 its damping efficiency. Moreover, paddle wave orbital motions de-phase Marangoni and gravity-capillary waves
 8 making the resonance-type damping due to the oil film less effective. These effects have impact also on the short
 9 wind waves, as the damping effect appears to cease at frequencies higher than 9 Hz (Figure 12)



10

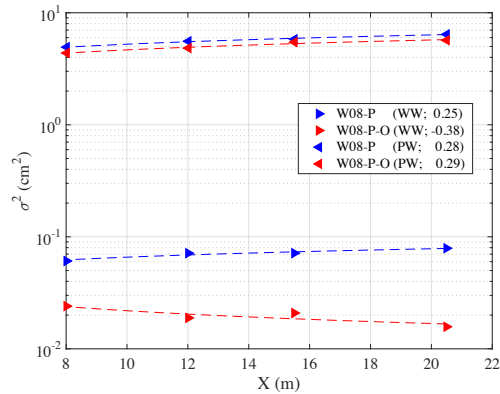
11 **Figure 11: Wave energy spectra $E(f_a)$ and $E(f_i)$ of the water surface elevation $z(t)$ at different fetches for the reference wind speed of 8**
 12 **m/s and irregular paddle waves. (left) Clean water experiment W08-P. (right) Water with oil experiment W08-P-O (the spectrum at**
 13 **the fetch $X = 20.5$ m is replicated with a blue dashed line on the left panel). On left panels, the black solid and dashed lines are the**
 14 **reference spectral shape proportional to f^4 and f^{-5} , respectively. On bottom panels the dashed gray vertical line shows the maximum**
 15 **frequency (2 Hz) produced by the paddle, and the vertical dotted black line on the bottom-right panel shows the fish oil resonance**
 16 **frequency $f_{res} = \omega_{res}/(2\pi) = 3.77$ Hz.**



1

2 **Figure 12: Damping of the wave energy for oil-covered water surface. The damping coefficient is evaluated as the ratio $D = E_o / E_c$**
3 **between the variance density spectrum of the water surface elevation with oil slick (E_o ; experiment W08-P-O) and in clean water (E_c ;**
4 **experiment W08-P). The black solid line is the average shape of the damping coefficient (for the sake of clarity the series is smoothed**
5 **with a moving average procedure). The solid black line shows the level $E_o = E_c$.**

6 Similarly to what was done for the only wind-wave case (Figure 7), it is instructive to check the small
7 difference of energy (in practice wave height) with fetch of the two basic components (paddle and wind waves) of
8 the spectra in clean water and in water with oil. The differences are tiny, and barely visible in Figure 13. Because
9 of the partial superposition of the two (paddle and wind) frequency ranges, we have computed, for the intrinsic
10 spectra, the surface elevation variance below 1.3 Hz (PW in Figure 13, dominated by paddle waves) and above 2
11 Hz (WW in Figure 13, dominated by wind waves). For the high-frequency part of the wind wave spectrum, in clean
12 water, waves grow slightly with fetch, gaining 30% energy passing from $X = 8$ m fetch to $X = 20.5$ m. The growth
13 is obviously much smaller than in absence of swell, but still there is a bit. The presence of oil (red marker) makes
14 the waves progressively decreasing with fetch (the coefficient $\beta < 0$), consistently with, and with the same
15 explanation for, the results obtained without paddle waves.



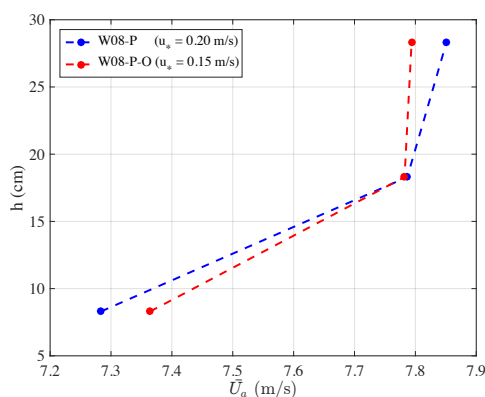
1

2 **Figure 13: Spatial evolution of the water surface elevation variance σ^2 of co-existing wind (WW) and paddle (PW) waves in clean**
3 **water (W08-P) and with oil slick (W08-P-O). The solid and dashed lines show the power law-type function fitting the experimental**
4 **data. In the legend the coefficient β of the fitted power law is shown.**

5 The growth of paddle waves (swell) is particularly interesting because it appears to be marginally affected
6 by the presence of oil (PW markers in Figure 13), similar to the result found by Mitsuyasu and Honda (1986) using
7 monochromatic paddle waves. We interpret this saying that the reduction of surface roughness between the two
8 panels in Figure 9 is not sufficient to change substantially the vertical profile of the turbulent airflow, hence the
9 generation process acting on swell. This is confirmed by Figure 14 that shows the wind profile with and without
10 oil. There is only a small difference between the two cases (however the friction velocity is, as expected, larger in
11 clean water). This implies that the minor disturbances we see in the right panel of Figure 9 suffice for making the
12 wind feel the surface as rough. Indeed we are here at the limit because the further, almost complete, wave reduction
13 we see in Figure 2 for the experiment W06-O changes dramatically the wind profile, as already seen in Figure 3.

14

15



1

2 **Figure 14:** Vertical profile of the measured mean horizontal wind speed \bar{U}_a measured over the water surface at fetch $X = 11.5$ m for
3 co-existing wind- and paddle-generated waves in clean water condition (blue) and after the oil instillation (red). In the legend, the
4 value of the friction velocity is shown within brackets. Only the value recorded at the three lowest Pitot tubes are shown.

5 4 Discussion

6 Our previous description of the general methodology and results has been focused much on the implications of
7 having the water surface covered by a very thin (10^{-8} m) layer of fish oil. However interesting in itself, it is clear
8 that the main virtue of these experiments has been the opening of a different perspective on the physics of air-sea
9 interactions. We discuss here the main suggestions and ideas derived from our results.

- 10 – The different wind profile and wave growth without and with oil clearly show that the stress felt by the
11 atmosphere is, as anticipated by Janssen (1991), the sum of the friction stress and the input to waves. Lacking
12 the latter, the atmospheric stress reduces to the purely frictional one. This has implications also for circulation
13 modeling where quite often the wave intermediate role (wind input to waves followed by wave input to current
14 via breaking) is by-passed by an artificially inflated surface friction to current. Janssen (1991) added wave
15 growth to the stress felt by the atmosphere. McWilliams and Restrepo (1999) showed how the general global
16 circulation could be obtained also driving it only with breaking waves. Our experiments have shown what τ_a
17 reduces to if waves do not appear. We can argue about a possibly increased friction drag in presence of a rough
18 surface, but the general principle remains.
- 19 – Especially with young, hence relatively slow, waves it is essential to consider generation with respect to the
20 surface current. In our case, lacking any instrument to measure current, and in particular its vertical profile, we



1 have used two independent methods based on video documentation to get an estimate of the surface current
2 drift. The two approaches provided similar results, consistent with that derived from the wind speed and similar
3 conditions in the literature. Lacking any data on the current vertical profile, and supported also by the
4 recirculation characteristics of the wave tank, we made the blunt assumption of a vertically uniform current.
5 This is a first order approximation, acceptable in our case because the related discussion concerns only very
6 short waves. In any case, stated in the final summary, more complete experiments are planned for the near
7 future.

8 – We have found it fascinating to look at how the water surface reacts and evolves under the action of an
9 impulsive wind forcing. As with oil, there is a lot to learn from these first stages of evolution of a wave field.
10 For this first analysis of the obtained data, we have limited ourselves to the steady, fetch-limited conditions
11 where we already found plenty of material for arguing and discussion. Our next step will be in the transient
12 area. However, this subject takes us to a very short discussion on the generation mechanism(s) of the earliest
13 waves. In this respect, the spectral approach to wind wave modeling began with the study by Pierson et al.
14 (1955), followed by the two parallel and independent, but complementary, papers by Phillips (1957) and Miles
15 (1957), and the definition of the energy balance equation by Gelci et al. (1957). While the Miles' mechanism,
16 refined by Janssen (1991), provides the bulk of the input to waves, we still need to trigger the first wavelets on
17 which Miles, and non-linear interactions, can then act. Two processes compete for this first stage: the just
18 mentioned one by Phillips, associated to assumed pressure oscillations moving with the wind, supported also
19 by the recent paper by Zavadsky and Shemer (2017), and a sort of Kelvin-Helmoltz instability (Kawai, 1979)
20 due to the strong vertical shear in the surface water layer following the initial action by wind. The matter is not
21 relevant for practical purposes because these initial stages are usually parameterized or bypassed in wave
22 modeling in a pragmatic way. We know these wavelets appear and their exact dimensions are irrelevant for the
23 following evolution of the actual field. However, our experiments provide a small piece of information. The
24 Phillips' mechanism is supposed to act on any wavelength, independently of the other ones. We argue that in
25 the oily experiment, granted the dissipation at the wavelet scale due to the Marangoni effect, nothing would
26 impede the Phillips' mechanism to act on the longer waves. However, we found no evidence of energy in the
27 corresponding wave components.



1 – With wind and swell, the presence of oil still reduces wind-wave generation but there is more wind-wave
2 energy than with only wind. Therefore we can say that the presence of a swell reduces the effectiveness of the
3 oil in impeding local generation. We hypothesize this is due to the very thin, almost mono-molecular, layer of
4 oil we used and to the swell orbital stretching continuously disrupting the continuity of the oil layer, hence the
5 effectiveness of the Marangoni forces.

6 **5 Conclusion and summary**

7 With the help of an experimental facility, we studied the influence of a very thin layer of fish oil (acting as
8 surfactant) on wind and paddle waves as well as on the parameters of the lowest airflow layer. Measurements of
9 sea surface elevation at different fetches and of wind speed were carried out in both clean water (acting as reference
10 condition) and in water with fish oil (producing a viscoelastic film on the surface). The damping of short gravity-
11 capillary waves by surfactants appears a convenient condition to study, to a large scale, the processes of interaction
12 between the water body and the atmosphere. The aim of the present study is thus to evaluate the influence of the oil
13 film on the frequency spectrum and growth of wind and paddle waves and on some parameters of the interaction of
14 the water body with the atmosphere. Taking this viewpoint, principal conclusions of our study can be summarized
15 as follows:

- 16 – Marangoni forces, associated to the presence of the fish oil, quickly dissipate and impede the formation of the
17 first wavelets, hence, in a laboratory, the growth of any wind sea. As it is generally agreed, this dissipation at
18 short wavelengths leads to an intensified energy transfer via non-linear interactions from the bulk of the
19 spectrum, in so doing not only smoothing, but also partly calming the sea. In the fish-oil covered wave tank,
20 the powerful suppression of the first wavelets leaves the airflow vertical profile unaffected by the wave field,
21 so that the Miles-Janssen wave growth mechanism is not triggered.
- 22 – Our results show the efficacy of the fish oil in suppressing the wave generation by wind. Indeed, in the
23 experiments in a wind-wave tank contaminated by non-animal surfactants, Hühnerfuss et al. (1981) found that
24 the peak of the spectra is shifted towards higher frequency in reference to the peak frequency in clean water.
25 However, a wind-wave spectrum was still present in their tests, whilst we have found that using fish oil in the
26 wind-only condition (reference wind speed of 6 m/s) the wave field does not grow from the rest condition,
27 leading to a strong modification of the airflow vertical profile.



1 – The experiment with wind-wave only in water with fish oil (experiment W06-O) gave us the unique
2 opportunity to investigate (albeit preliminarily) the interactions at the air-water interface in absence of surface
3 waves. Clearly, the stress exerted in that case by the airflow is smaller than the one in clean water (when the
4 wave field regularly develops) and the water current is determined by the wind shear only, so that $\tau_w \approx \tau_a$.
5 This condition is expected to be different from the one obtained for fully developed waves (in clean water),
6 when one should find that in Eq. (10) the momentum flux into the water column τ_w should become the
7 atmospheric stress τ_a as the wave field reaches equilibrium (see ECMWF, 2017). For instance, the water
8 current vertical profile below the surface is expected to be different in clean water and in water with oil. In this
9 respect, new experiments are already planned that will investigate also the drift current distribution beneath the
10 water surface for an oil-covered water surface.

11 – The strong wave damping by oil in pure wind sea conditions is less so in presence of swell. We ascribe this to
12 the continuous stretching of the surface due to swell and the consequent decrease of the effectiveness of the
13 Marangoni forces.

14 – The growth of paddle (relatively) long waves seems to be little affected by the roughness of short waves.
15 Provided a minimal background of very short waves (in practice surface roughness) is present, the growth of
16 paddle waves under the action of wind is largely independent on the background level, a fact we ascribe to the
17 similar distortion of the wind profile in the two cases.

18 As mentioned in the text, we have barely (and literally) touched the surface of the subject. Wave generation and
19 dissipation, and more general atmosphere and sea dynamic interaction, are still to be fully explored. The approach
20 we followed, experiments in a wind wave tank without and with oil on the surface, offers new possibilities for
21 explaining this old, but still fruitful, field.

22 **Appendix A: Surface current drift estimate using optical flow**

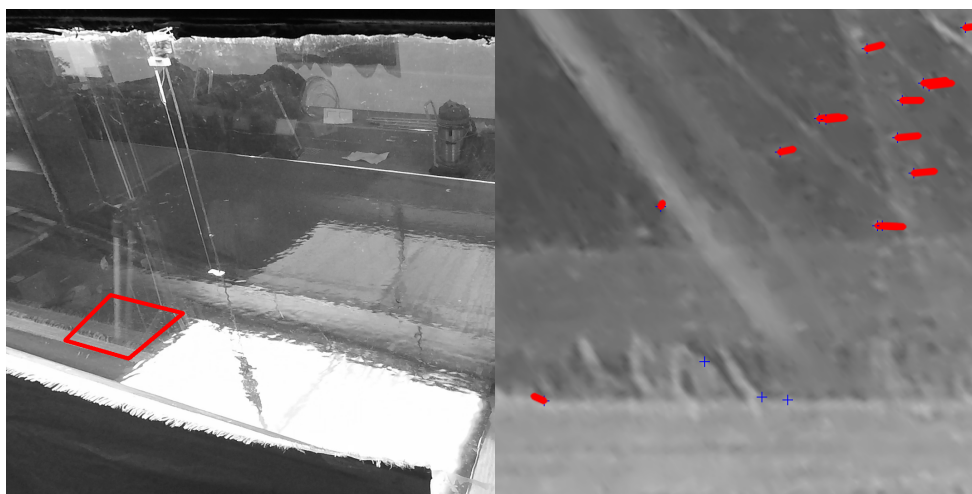
23 As it is specified in Section 3.1.1, tiny bubbles moving on the surface along the tank, and visible in the 1920x1080
24 pixel images captured at 60 Hz by a video-camera placed outside the tank close to prove G4, made it possible to
25 have an estimate of the surface current. The probe's two vertical wires, whose measures have been accurately
26 determined, were used to map visual features from the image space (in pixels) to the tank surface space (in meters).
27 To ease the computation, we manually defined a quadrilateral area in the image and computed the homographic



1 transformation between the quadrilateral space to a normalized rectangular space of size 512x512 pixels. To
2 account for the possible uneven illumination along the sequence, each image was normalized so that the intensity
3 values have zero mean and unitary standard deviation. Due to the optical characteristics of the water, bubbles are
4 not the only visual features present in the frames. Indeed, visual clutter mostly due to reflections makes it more
5 complex to reliably track the bubbles during the whole sequence. Since the cameras were firmly placed on a tripod
6 during the acquisition, and light conditions were mostly controlled, the clutter appearance remains quite stable
7 among the frames, with slight fluctuations due to the small waves and the automatic exposure adjustments of the
8 camera.

9 Therefore, we performed a simple background subtraction by computing the squared difference between
10 each frame and the frame obtained by averaging the intensity values of the previous 3 frames. To remove the high-
11 frequency noise and artifacts caused by video compression, we blurred the background-subtracted image with a
12 3x3 Gaussian kernel and applied a threshold of 1.8 to obtain binary images. From the binary image of each frame,
13 we extracted the location of each particle by using the function *goodFeaturesToTrack()* provided by the OpenCV
14 Computer Vision Library (Bradski and Kaehler, 2008). We specified 2000 max corners, a quality level of 0.08, a
15 minimum distance between features of 3 pixels and a block size of 9x9 pixels. Then, we computed the sparse
16 optical flow with respect to the subsequent frame at the location of each particle using the iterative Lucas-Kanade
17 method with pyramids provided by OpenCV. We used a 15x15 pixels window for the matching and a pyramid
18 depth of 5 levels. The computed optical flow gives the amount of movement performed by each tracked particle
19 between each frame (Figure 15). By knowing the mapping between pixels and tank metric space, and the camera
20 frame rate, we could estimate the speed (in m/s) of each particle. So, we transformed particle locations and
21 movement vectors back to the original image space by inverting the homography.

22



1

2 **Figure 15:** Estimate of surface current speed by optical flow during experiment W06-O. (left) Bounded by a red polygon, the surface
3 area used for the determination of the flow. (right) Example of detected particles with their corresponding movement vector. The
4 wind was blowing from the left side to the right side of the images.

5 **Supplementary Material (Videos)**

6 1. Supplementary material SM1 available at <https://doi.org/10.5281/zenodo.1434262>.

7 2. Supplementary material SM2 available at <https://doi.org/10.5281/zenodo.1434272>.

8 **Author contributions.** All authors have contributed to the writing of the paper. Experiments were planned
9 by LC and FQ, and executed by all authors. Data analysis and interpretation were performed by AB with the help
10 of LC, FB, and SJ.

11 **Competing interests.** The authors declare that they have no conflict of interest.

12 **Acknowledgements**

13 Authors gratefully acknowledge the funding from the Flagship Project RITMARE - The Italian Research for the
14 Sea - coordinated by the Italian National Research Council and funded by the Italian Ministry of Education,
15 University and Research within the National Research Program 201115. The authors are pleased to acknowledge
16 useful discussions with P.A.E.M Janssen, Norden Huang, Jean-Raymond Bidlot, and Francesco Barbariol. Luigi
17 Cavaleri has been partially supported by the EU contract 730030 call H2020-EO-20116 'CEASELESS'.

18



1 References

- 2 Adrian, R. J.: Particle-Imaging Techniques For Experimental Fluid Mechanics, *Annu. Rev. Fluid Mech.*, 23, 261–
3 304, 1991.
- 4 Alpers, W. and Hühnerfuss, H.: The damping of ocean waves by surface films: A new look at an old problem, *J.*
5 *Geophys. Res.*, 94(C5), 6251–6265, doi:10.1029/JC094iC05p06251, 1989.
- 6 Benetazzo, A., Bergamasco, F., Yoo, J., Cavaleri, L., Kim, S., Bertotti, L., Barbariol, F. and Shim, J.:
7 Characterizing the signature of a spatio-temporal wind wave field, *Ocean Model.*, 129, 104–123,
8 doi:10.1016/j.ocemod.2018.06.007, 2018.
- 9 Bradski, G. and Kaehler, A.: *Learning OpenCV: Computer Vision with the OpenCV Library*, edited by Or. M. Inc.,
10 2008.
- 11 Buckley, M. P. and Veron, F.: Structure of the Airflow above Surface Waves, *J. Phys. Oceanogr.*, 46(5), 1377–
12 1397, doi:10.1175/JPO-D-15-0135.1, 2016.
- 13 Chen, G. and Belcher, S. E.: Effects of long waves on wind-generated waves, *J. Phys. Oceanogr.*, 30(9), 2246–
14 2256, 2000.
- 15 Cini, R., Lombardini, P. P. and H.: Remote sensing of marine slicks utilizing their influence on wave spectra, *Int. J.*
16 *Remote Sens.*, 4(1), 101–110, 1983.
- 17 Cox, C. S., Zhang, X. and Duda, T. F.: Suppressing breakers with polar oil films: Using an epic sea rescue to model
18 wave energy budgets, *Geophys. Res. Lett.*, 44, 1414–1421, doi:10.1002/2016GL071505., 2017.
- 19 Donelan, M. A.: The effect of swell on the growth of wind waves, *Johns Hopkins APL Tech. Dig.*, 8(1), 18–23,
20 doi:10.1016/S0422-9894(08)70110-7, 1987.
- 21 Donelan, M. A.: Air-sea interaction, in *The Sea*, vol. 9, *Ocean Engineering Science*, edited by B. LeMehaute and
22 D. M. Hanes, pp. 139–292, Wiley-Interscience, Hoboken, N. J. (USA), 1990.
- 23 Donelan, M. A., Haus, B. K., Plant, W. J. and Troianowski, O.: Modulation of short wind waves by long waves, *J.*
24 *Geophys. Res.*, 115(C10003), 1–12, doi:10.1029/2009JC005794, 2010.
- 25 ECMWF: PART VII: ECMWF WAVE MODEL, in *IFS Documentation CY43R3*, p. 99, ECMWF. [online]
26 Available from: <https://www.ecmwf.int/en/elibrary/17739-part-vii-ecmwf-wave-model>, 2017.
- 27 Ermakov, S. A., Panchenko, A. R. and Talipova, T. G.: Damping of High-frequency Wind Waves by Artificial
28 Surface-active Films., *Izv. Akad. Nauk SSSR. Fiz. Atmos. i okeana*, 21, 54–58, 1985.
- 29 Ermakov, S. A., Zujkova, A. M., Panchenko, A. R., Salashin, S. G., Talipova, T. G. and Titov, T. I.: Surface film
30 effect on short wind waves, *Dyn. Atmos. Ocean.*, 10, 31–50, 1986.
- 31 Fairall, C. W., Bradley, E. F., Hare, J. E., Grachev, A. A. and Edson, J. B.: Bulk Parameterization of Air–Sea
32 Fluxes: Updates and Verification for the COARE Algorithm, *J. Phys. Oceanogr.*, 16(4), 571–591, 2003.
- 33 Feindt, F.: Radar-Rfickstreueexperimenteam Wind-Wellen-Kanal bei sauberer und filmbedeckter Wasseroberfläche
34 im X-Band (9.8 GHz), Ph.D.thesis, Univ.of Hamburg, Federal Republic of Germany., 1985.
- 35 Fiscella, B., Lombardini, P. P., Trivero, P. and Cini, R.: Ripple Damping on Water Surface Covered by a Spreading
36 Film : Theory and Experiment, *Nuovo Cim.*, 8(5), 491–500, 1985.
- 37 Foda, M. and Cox, C. S.: The spreading of thin liquid films on a water-air interface, *J. Fluid Mech.*, 101, 33–51,
38 1980.
- 39 van Gastel, K., Janssen, P. A. E. M. and Komen, G. J.: On phase velocity and growth rate of wind-induced gravity-
40 capillary waves, *J. Fluid Mech.*, 161, 199–216, doi:10.1017/S0022112085002889, 1985.
- 41 Gelci, R., Cazalé, J. and Vassal, J.: Prévission de la houle. La méthode des densités spectroangulaires, *Bull. Inform.*
42 *Com. Cent. Ocean. D’Etude Cotes*, (9), 416–435, 1957.
- 43 Hasselmann, K.: On the non-linear energy transfer in a gravity-wave spectrum Part 1. General theory, *J. Fluid*
44 *Mech.*, 12(4), 481–500, doi:10.1017/S0022112062000373, 1962.



- 1 Hühnerfuss, H., Alpers, W., Lange, P. . and Walter, W.: Attenuation of wind waves by artificial surface films of
2 different chemical structure, *Geophys. Res. Lett.*, 8(11), 1184–1186, 1981.
- 3 Hühnerfuss, H., Alpers, W., Garrett, D., Lange, P. . and Stolte, S.: Attenuation of capillary and gravity waves at sea
4 by monomolecular organic surface films, *J. Geophys. Res.*, 88, 9809–9816, 1983.
- 5 Hwang, P. A., García-Nava, H., Ocampo-Torres, F. J., Hwang, P. A., García-Nava, H. and Ocampo-Torres, F. J.:
6 Observations of Wind Wave Development in Mixed Seas and Unsteady Wind Forcing, *J. Phys. Oceanogr.*, 41(12),
7 2343–2362, doi:10.1175/JPO-D-11-044.1, 2011.
- 8 Janssen, P.: Quasi-linear Theory of Wind-Wave Generation Applied to Wave Forecasting, *J. Phys. Oceanogr.*,
9 21(11), 1631–1672, 1991.
- 10 Janssen, P. A. E. M.: Quasilinear approximation for the spectrum of wind-generated water waves, *J. Fluid Mech.*,
11 117, 493–506, 1982.
- 12 Janssen, P. A. E. M. and Bidlot, J.-R.: Progress in in Operational Operational Wave Wave Forecasting, *Procedia*
13 *IUTAM*, 26, 14–29, 2018.
- 14 Kawai, S.: Generation of initial wavelets by instability of a coupled shear flow and their evolution to wind waves,
15 *J. Fluid Mech.*, 93(4), 661–703, doi:10.1017/S002211207900197X, 1979.
- 16 Kirby, J. T. and Chen, T. M.: Surface-waves on vertically sheared flows: approximate dispersion relations., *J.*
17 *Geophys. Res. Ocean.*, 94(C1), 1013–1027, 1989.
- 18 Komen, G. J., Cavaleri, L., M. Donelan, K. H., Hasselmann, S. and Janssen, P. A. E. M.: *Dynamics and Modelling*
19 *of Ocean Waves.*, edited by Cambridge University Press, Cambridge University Press., 1994.
- 20 Kusaba, T. and Mitsuyasu, H.: Wind-induced growth of water waves with dual wave components, (Preliminary
21 report), 60, 455–466, 1984.
- 22 Liberzon, D. and Shemer, L. E. V: Experimental study of the initial stages of wind waves ' spatial evolution, *J.*
23 *Fluid Mech.*, 681, 462–498, doi:10.1017/jfm.2011.208, 2011.
- 24 Lindgren, G., Rychlik, I. and Prevosto, M.: Stochastic Doppler shift and encountered wave period distributions in
25 Gaussian waves, *Ocean Eng.*, 26, 507–518, 1999.
- 26 Longuet-Higgins, M. S.: The effect of nonlinearities on statistical distribution in the theory of sea waves, *J. Fluid*
27 *Mech.*, 17(3), 459–480, 1963.
- 28 Longuet-Higgins, M. S. and Stewart, R. H.: Changes in the form of short gravity waves on long waves and tidal
29 currents, *J. Fluid Mech.*, 8(4), 565–583, 1960.
- 30 Marangoni, C.: Sul principio della viscosità superficiale dei liquidi stabili, *Nuovo Cimento*, Ser. 2, 5/6, 239–273,
31 1872.
- 32 McWilliams, J. C. and Restrepo, J. M.: The Wave-Driven Ocean Circulation, *J. Phys. Oceanogr.*, 29(10), 2523–
33 2540, doi:10.1175/1520-0485(1999)029<2523:TWDOC>2.0.CO;2, 1999.
- 34 Miles, J.: Surface-wave generation revisited, *J. Fluid Mech.*, 256, 427–441, 1993.
- 35 Miles, J. W.: On generation of surface waves by shear flows, *J. Fluid Mech.*, 3, 185–204, 1957.
- 36 Mitsuyasu, H.: Interactions between water waves and winds (1). Rep. Research Inst. Appl. Mech. (RIAM), Kyushu
37 Univ. 14 (48)., 1966.
- 38 Mitsuyasu, H.: Reminiscences on the study of wind waves, *Proc. Jpn. Acad.*, Ser. B, 91(4), 109–130, 2015.
- 39 Mitsuyasu, H. and Honda, T.: Wind-induced growth of water waves, *J. Fluid Mech.*, 123, 425–442,
40 doi:10.1017/S0022112082003139, 1982.
- 41 Mitsuyasu, H. and Honda, T.: The effects of surfactant on certain air-sea interaction phenomena, in *Wave*
42 *Dynamics and Radio Probing of the Ocean Surface*, pp. 41–57, Held May 13-20, 1981, in Miami, Florida. Edited
43 by O. M. Phillips and K. Hasselmann, pp. 41-57, Plenum, New York., 1986.
- 44 Peirson, W. L.: Measurement of surface velocities and shears at a wavy air-water interface using particle image
45 velocimetry, *Exp. Fluids*, 23, 427–437, 1997.



- 1 Phillips, O. M.: On the generation of waves by turbulent wind, *J. Fluid Mech.*, 2, 417–445, 1957.
- 2 Phillips, O. M. and Banner, M. L.: Wave breaking in the presence of wind drift and swell., *J. Fluid Mech.*, 66, 625–
3 640, 1974.
- 4 Pierson, W. J., Neumann, G. and James, R. W.: Practical Methods for Observing and Forecasting Ocean Waves by
5 Means of Wave Spectra and Statistics, Washington, U.S. Navy Hydrogr. Off. Publ. No. 603, 284 pp, 1955.
- 6 Steinman, D. B.: Problems of aerodynamic and hydrodynamic stability, in 3rd Hydrulic Conference. Studies in
7 Engineering, Bull. No. 31., 1946.
- 8 Stewart, R. H. and Joy, W. J.: HF radio measurements of surface currents, *Deep. Res.*, 21, 1039–1049, 1974.
- 9 Welch, P. D.: The Use of Fast Fourier Transform for the Estimation of Power Spectra: A Method Based on Time
10 Averaging Over Short, Modified Periodograms, *IEEE Trans. Audio Electroacoust.*, AI-15(2),
11 doi:10.1109/TAU.1967.1161901, 1967.
- 12 Wu, J.: Wind-induced drift currents, *J. fluid*, 6(1), 49–70, 1975.
- 13 Zavadsky, A. and Shemer, L.: Water waves excited by near-impulsive wind forcing, *J. Fluid Mech.*, 828, 459–495,
14 doi:10.1017/jfm.2017.521, 2017.
- 15